# Tanzania Journal of Science

Volume 51(3), 2025





# Nickel (II) complex decorated zinc-cadmium sulfide type-II heterojunction for enhanced photocatalytic hydrogen production

Miza Kombo, 1\*Abdul Muhamed, 1 Suleiman Suleiman, 2 and An-Wu Xu3

### **Keywords**

Zn<sub>0.5</sub>Cd<sub>0.5</sub>S/NPBIm; Type-II heterostructure; Hydrogen production; Visible-light; Semiconductor; photocatalysts

### **Abstract**

The binary metal sulfide Zn<sub>0.5</sub>Cd<sub>0.5</sub>S has emerged as a promising photocatalyst for hydrogen (H<sub>2</sub>) production via visible-light-driven water splitting. However, its practical application is limited by rapid charge carrier recombination and insufficient stability. In this study, nickel (II)-(3-pyridyl) benzimidazole (NPBIm) complexes were synthesized and employed an ultrasonic-assisted method to decorate the surface of  $Zn_{0.5}Cd_{0.5}S$ , forming novel metal-complex a heterostructure system ( $Zn_{0.5}Cd_{0.5}S/NPBIm$ ). This hybrid system significantly enhances photocatalytic H<sub>2</sub> evolution under visible light irradiation. Experimental findings reveal that the incorporation of NPBIm molecules improves the optical absorption of Zn<sub>0.5</sub>Cd<sub>0.5</sub>S and facilitates more efficient separation and migration of photogenerated charge carriers. The optimized Zn<sub>0.5</sub>Cd<sub>0.5</sub>S/NPBIm hybrid heterostructure exhibits a remarkable hydrogen production rate of 272.22 µmol h<sup>-1</sup> under visible light irradiation ( $\lambda \ge 420$  nm), which is more than three times higher than that of pure Zn<sub>0.5</sub>Cd<sub>0.5</sub>S (92.54 µmol h<sup>-1</sup>). This significant enhancement demonstrates the potential of combining semiconductor materials with metal-complex structures to improve photocatalytic performance. Furthermore, the hybrid photocatalyst exhibits excellent stability, an essential criterion for long-term energy applications. These findings highlight the effectiveness of integrating semiconductor materials with metal-complex structures to enhance photocatalytic performance. This study contributes to the advancement of solar-driven hydrogen production and offers a promising strategy for developing next-generation photocatalysts, with broader relevance to renewable energy and environmental sustainability.

### Introduction

Nowadays, hydrogen is considered an ideal alternative energy source for fossil fuels due to its high energy content, renewability, and environmentally friendly nature (Chen et al.

2024, Yuan et al. 2022). However, producing hydrogen  $(H_2)$  in a simple, efficient and sustainable manner remains a significant challenge. Photocatalytic hydrogen production offers a green route to convert

Received March 2025, Revised August 2025, Accepted 19 October 2025, Published 30 October 2025  $\frac{\text{https://doi.org/10.65085/2507-7961.1058}}{\text{https://doi.org/10.65085/2507-7961.1058}}$ 

© College of Natural and Applied Sciences, University of Dar es Salaam, 2025 ISSN 0856-1761, e-ISSN 2507-7961

<sup>&</sup>lt;sup>1</sup>Department of Natural Science, School of Natural and Social Sciences, The State University of Zanzibar. P. O. Box 146. Zanzibar-Tanzania

<sup>&</sup>lt;sup>2</sup>Tanzania Atomic Energy Commission, Directorate of Radiation Control, P.O. Box 1520, Mwanza, Tanzania.
<sup>3</sup>Division of Nanomaterials and Chemistry, Hefei National Laboratory for Physical Sciences at the Microscale, Department of Chemistry Physics, University of Science and Technology of China, Hefei, 230026, People's Republic of China.

<sup>\*</sup>Corresponding author: miza.kombo@suza.ac.tz

solar energy into chemical energy via water splitting, a method first demonstrated using a TiO<sub>2</sub> electrode by Fujishima and Honda in 1972 (Fujishima and Honda 1972). Since then, extensive efforts have focused on developing efficient semiconductor photocatalysts for this purpose. Various materials have been explored, including metal sulfides (Mamiyev and Balayeva 2022), metal oxides (Grushevskaya et al. 2022), and carbon nitrides (Tahir et al. 2022). Among these, metal sulfides stand out for favorable optical and electronic properties under visible light (Bai et al. 2021 and Mamiyev and Balayeva 2022). In particular, the binary solid solution Zn<sub>x</sub>Cd<sub>1-x</sub>S has attracted attention due to its tunable bandgap, achieved by adjusting the Zn/Cd ratio between the narrow-bandgap CdS (2.4 eV) and wide-bandgap ZnS (3.6 eV) (Hamdan et al. 2024 and Qi et al. 2021). This tunability enhances visible-light absorption and optimizes energy levels for water splitting.

Despite these advantages,  $Zn_xCd_{1-x}S$  suffers from a rapid recombination of photogenerated charge carriers, which limits its photocatalytic efficiency (Gan et al. 2021). To overcome this, strategies such as forming heterojunctions with other semiconductors have been employed to improve charge separation and transfer (Bai et al. 2021, Gan et al. 2021 and Lei et al. 2021). Additionally, previous studies demonstrated that modifying semiconductors with appropriate organic molecules could facilitate more efficient charge transport through ligand bridging or  $\pi$ - $\pi$  interactions (Kombo et al. 2020).

One such promising molecule is Nickel (II)-3-pyridyl benzimidazole (NPBIm), an organometallic polymer with an imidazole ring and extended  $\pi$ -conjugation. This structure allows for hydrogen bonding and  $\pi$ - $\pi$  stacking interactions which enhancing its optical absorption and electron transport capabilities (Icli et al. 2009, Su et al. 1999 and Wei et al. 2014). The ligand 2-(3-pyridyl) benzimidazole (PBIm) also supports coordination with various metals, forming supramolecular architectures (Geng et al. 2012 and Wei et al. 2014). Therefore, NPBIm is an ideal material that could be merged with  $Zn_{0.5}Cd_{0.5}S$  photocatalyst to form a type-II heterostructured photocatalyst ( $Zn_{0.5}Cd_{0.5}S/NPBIm$ ), thus could promote the separation of photogenerated charge carriers, and then enhance the photocatalytic  $H_2$  production performance.

This work represents a meaningful advancement in the field of photocatalysis by introducing an innovative organic-inorganic hybrid heterostructure that significantly enhances hydrogen production under visible light. Unlike previous studies that have largely focused on metal sulfide-based binary systems or inorganic cocatalysts, this study employs a Nickel (II)-based organic complex (NPBIm) to modify Zn<sub>0.5</sub>Cd<sub>0.5</sub>S, forming a type-II heterojunction that improves charge carrier separation and light absorption. The resulting composite  $Zn_{0.5}Cd_{0.5}S/NPBIm$ hybrid exhibited significantly enhanced photocatalytic H<sub>2</sub> production, achieving an optimal rate of 272.22 umol h-1 under visible light ( $\lambda \ge 420$  nm), approximately three times that of the unmodified Zn<sub>0.5</sub>Cd<sub>0.5</sub>S (92.54 μmol h<sup>-1</sup>). This system presents promising potential for large-scale development due to its use of inexpensive materials, applied a scalable synthesis route that avoids hightemperature and produce a stable material. These findings not only demonstrate a promising route for boosting photocatalytic hydrogen production but also offers a more environmentally friendly and cost-effective solution for solar fuel applications.

# Materials and Methods Chemicals and Reagents

Zinc acetate dihydrate (Zn(Ac)<sub>2</sub>.2H<sub>2</sub>O), cadmium acetate dihydrate (Cd(Ac)2.2H2O), sodium sulphide nonahydrate (Na<sub>2</sub>S.9H<sub>2</sub>O), sodium hydroxide (NaOH), sodium sulphite nitrate hexahydrate (Na<sub>2</sub>SO<sub>3</sub>),nickel  $(Ni(NO_3)_2.6H_2O)$  and methanol ( $\geq 99\%$ ) were purchased from Sinopharm Chemical Reagent Co., Ltd. Chloroplatinic hexahydrate ( $H_2PtCl_6 \cdot 6H_2O_1 \ge 37\%$  Pt basis) was bought from Aldrich and 2-(3-pyridyl) benzimidazole was obtained from Alfa Aesar (China) Chemicals Co., Ltd. All chemicals were of analytical grade, thus they were used

as received from the manufactures without further purification. Besides, the double distilled water used in all experiments was produced from a distillation apparatus (SZ-93A auto-double distillation apparatus, YaRong Corp., Shanghai, China).

### Preparation of Zn<sub>0.5</sub>Cd<sub>0.5</sub>S

Zn<sub>0</sub> 5Cd0 <sub>5</sub>S solid solution The fabricated by a one-step coprecipitation route at room temperature according to our previous work (Shen et al. 2017). In a typical synthesis, 3 mmol of zinc acetate dihydrate (Zn (Ac)<sub>2</sub>·2H<sub>2</sub>O) and 3 mmol of cadmium acetate dihvdrate (Cd(Ac)<sub>2</sub>·2H<sub>2</sub>O) were both dispersed in 50 mL of distilled water. Then, 0.2 M NaOH aqueous solution was applied to adjust the mixture to pH 7.3. After that, 9 mmol sodium sulphide nonahydrate (Na<sub>2</sub>S·9H<sub>2</sub>O) in 30 mL distilled water was added into the suspension drop wise, vellow precipitates gradually appeared. vigorous stirring, the yellow precipitation liquor was kept for 18 h at room temperature. Finally, the products were collected by centrifugation, washed with distilled water and absolute ethanol several times, and then dried at 80 °C for 6 h under vacuum.

### Preparation of NPBIm

Ni (II)-3-pyridyl benzimidazole (NPBIm) was prepared through solvothermal process. Typically, 5 mmol nickel nitrate hexahydrate (Ni (NO<sub>3</sub>)<sub>2</sub>.6H<sub>2</sub>O) was dissolved in 30 mL of methanol (CH<sub>3</sub>OH) to form a light green color solution. Meanwhile, in another beaker, 10 mmol 2-(3-pyridyl) benzimidazole was dissolved in 30 mL of CH<sub>3</sub>OH and stirring for 1 h to prepare a transparent solution. Later, the PBIm/CH<sub>3</sub>OH solution was quickly poured into the Ni<sup>2+</sup> solution. Mixed solution was again stirred for another 1 h, the resultant homogeneous solutions were transferred to a 100 mL Teflon-lined autoclave and then heated at 180 °C for 12 h in an oven. The obtained products were collected centrifugation, washed repeatedly with distilled water and ethanol three times and then dried at 60 °C in an oven prior to further analysis.

# $\begin{array}{lll} Preparation & of & Zn_{0.5}Cd_{0.5}S/NPBIm\\ Composite Photocatalysts & \end{array}$

The  $Zn_{0.5}Cd_{0.5}S/NPBIm$  composite photocatalyst was obtained by mixing an appropriate amount of NPBIm in  $Zn_{0.5}Cd_{0.5}S$  solution and the mixed solution was placed in the ultrasonic bath for 3 h, and then the product was dried for prior to use.

### Characterization

The crystal phase of the prepared samples Zn<sub>0.5</sub>Cd<sub>0.5</sub>S, NPBIm and Zn<sub>0.5</sub>Cd<sub>0.5</sub>S/NPBIm composite were characterized by powder Xray diffraction (XRD) measurements on Xray diffractometer (MXPAHF, Japan) with Cu K $\alpha$  irradiation ( $\lambda = 1.541$  Å) with an operating voltage of 40 kV and a current of 200 mA. The scanning angle was from 5° to 70°. The morphologies of the photocatalysts were observed by using a Transmission electron microscopy (TEM), on (JEOL-2010, Japan) at an accelerating voltage of 200 kV. The elemental composition and binding energies of the prepared catalysts were performed by using X-ray photoelectron spectroscopy (XPS) on ESCALAB 250 highperformance electron spectrometer, which was set to monochromated Al Kα radiation as the excitation source. The diffuse reflectance UV-vis absorption spectra of the photocatalysts were recorded by a Shimadzu spectrophotometer (Model 2501 PC). The steady-state photoluminescence (PL) spectra of samples were measured by using a fluorescence spectrophotometer (JY Fluorolog-3-Tau) with the wavelength at 325 nm. The time-resolved photoluminescence (TRPL) spectra were measured on a Laser Strobe Time-Resolved Spectrofluorometer (Photon Technology International (Canada) Inc.) with a USHIO xenon lamp source, 914 photomultiplier detection system a GL-302 and high-resolution dye laser (lifetimes 100 ps to 50 ms, excited by a Nitrogen laser). Brunauer-Emmett-Teller-specific surface area (SBET) was measured using N2 sorption isotherms at 77 K by an adsorption instrument (Micromeritics ASAP 2010 system) and the Brunauer-Emmett-Tellersspecific surface area (SBET) was calculated using a multi-point BET method.

### **Photoelectrochemical measurements**

The photocurrent response, electrochemical impedance spectroscopies (EIS) Nyquist plots and Mott-Schottky plots were measured CHI760E using electrochemical workstation (Chenhua Instrument Company, Shanghai, China) based on a standard threeelectrode system in which indium-tin oxide (ITO) glass as the working electrode, a saturated Ag/AgCl as the reference electrode, and Pt wire as the counter electrode. Na<sub>2</sub>SO<sub>4</sub> (0.5 M, 100 mL) was used as the electrolyte solution and a Xenon lamp (300 W) was used as a solar light source (( $\lambda \ge 420$  nm). For the preparation of working electrodes, 2 mg of either  $Zn_{0.5}Cd_{0.5}S$  or  $Zn_{0.5}Cd_{0.5}S/1$  wt% NPBIm samples were dispersed in 1 mL ethanol and 10 µL Nafion solution by ultrasonication process. The well-dispersed resulting mixture was spin-coated onto a piece of ITO glass (with a fixed area of ca. 1 cm<sup>2</sup>) and heated at 300 ° C for 2 h to remove organic species completely. electrochemical impedance spectroscopy (EIS) was recorded under visible light with a bias of -1 V and the frequency range was from 10 mHz to 100 kHz with an alternating current signal amplitude of 5 mV. The amperometric photocurrents were recorded by switch on/off event at a bias voltage of 0.5 V under visible light irradiation. The Mott-Schottky plots were obtained in the dark by scanning the electrode potential from -0.8 to and the impedance-potential characteristics were recorded at a frequency of 1 Hz.

## Photocatalytic hydrogen production

The photocatalytic  $H_2$  evolution from water splitting was carried out by using the outer Pyrex top-irradiation reaction vessel (500 mL), which is connected to a glass closed gas circulation system. During the experiment, 0.15 M Na<sub>2</sub>S·9H<sub>2</sub>O and 0.15 M Na<sub>2</sub>SO<sub>3</sub> serving as sacrificial reagents in an aqueous solution of 100 mL. 0.05 g of photocatalyst and different amounts of NPBIm were added into water. It was then kept in an ultrasonic bath for 30 min. The outer irradiation light source set on the top of the quartz window was a 300 W Xe lamp (Perfect Light, PLS-SXE300C, Beijing), which was equipped with a cut-off filter ( $\lambda \ge 420$  nm) to remove

ultraviolet light. Besides, the Pyrex reactor with a double layer was continuously stirred and cooled by running ethylene glycol. The photocatalytic reaction temperature was maintained at 5 °C. The average H<sub>2</sub> evolution rate of the photocatalysts during the first 4 hours was determined to evaluate the activities of the photocatalysts. The generated H<sub>2</sub> gas was analyzed using an online gas chromatograph (GC1120, Shanghai Sunny Hengping Limited, HTCD detector, N<sub>2</sub> as the carrier gas). After the completion of the reaction, photocatalysts (mixture Zn<sub>0.5</sub>Cd<sub>0.5</sub>S and NPBIm) were isolated from solution for reaction characterization. The catalysts are denoted as  $Zn_{0.5}Cd_{0.5}S/x$  NPBIm, where x 0.5, 1, and 1.5 wt% refers to the weight content of NPBIm in Zn<sub>0.5</sub>Cd<sub>0.5</sub>S/NPBIm composites.

### **Results and discussion**

Typically, Zn<sub>0.5</sub>Cd<sub>0.5</sub>S solid solution was synthesized by coprecipitation method at room temperature, and Ni (II)-3-pyridyl benzimidazole (NPBIm) was synthesized by a solvothermal route (Figure 1a). The NPBIm molecule was decorated on the surface of Zn<sub>0.5</sub>Cd<sub>0.5</sub>S via the ultrasonic method, and the Zn<sub>0.5</sub>Cd<sub>0.5</sub>S/NPBIm metal-complex semiconductor heterostructured photocatalysts with different weight contents of NPBIm were obtained (see Experimental Section). The X-ray diffraction (XRD) has been carried out to investigate the phase crystallinity and purity of the prepared samples. As displayed in Figure  $Zn_{0.5}Cd_{0.5}S$  solid solution shows three prominent broad diffractions peaks at 27.6°, 45.7°, and 53.8°, corresponding to (111), (220) and (311) crystal faces, respectively, well matching with the standard peaks of cubic zinc blende phase reported previously (Du et al. 2015 and Shen et al. 2017). No other peaks were found for impurities, demonstrating the high purity of the obtained Zn<sub>0.5</sub>Cd<sub>0.5</sub>S sample. After introducing NPBIm molecule onto the Zn<sub>0.5</sub>Cd<sub>0.5</sub>S photocatalyst, the XRD patterns of Zn<sub>0.5</sub>Cd<sub>0.5</sub>S/1 wt% NPBIm heterostructured photocatalyst similar to those of Zn<sub>0.5</sub>Cd<sub>0.5</sub>S, indicating that loading of NPBIm molecule has a negligible effect on the crystal phase of Zn<sub>0.5</sub>Cd<sub>0.5</sub>S. However, there is no any diffraction peaks of NPBIm detected in the Zn<sub>0.5</sub>Cd<sub>0.5</sub>S/NPBIm composite by XRD patterns, likely due to the very low content (1 wt %) in composites. The absence of sharp and well-defined peaks suggests that the material may be partially amorphous,

lacking the long-range order characteristic of crystalline substances. As a result, it does not exhibit sharp diffraction peaks. The presence of NPBIm molecule in the composites can be easily shown by XPS analysis as discussed later.

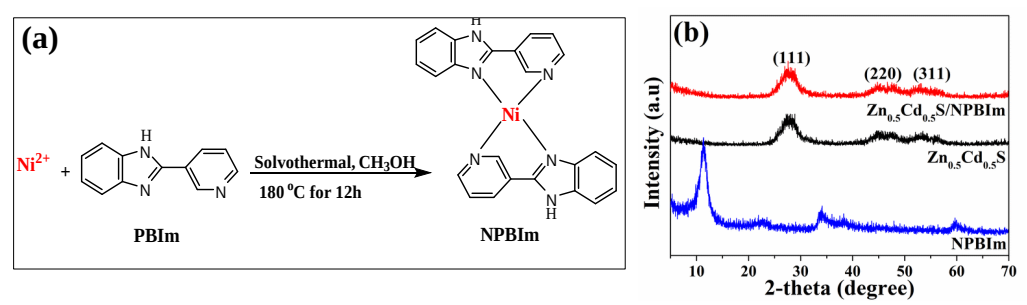


**Figure 1:** (a) Schematic illustration of the generation of the NPBIm coordination polymer based on Ni<sup>2+</sup> and 2-(3-pyridyl) benzimidazole (PBIm) ligand (b) XRD patterns of the NPBIm molecule,  $Zn_{0.5}Cd_{0.5}S$  and  $Zn_{0.5}Cd_{0.5}S/1$  wt% NPBIm photocatalyst.

The morphology of NPBIm molecule, pure  $Zn_{0.5}Cd_{0.5}S$  and  $Zn_{0.5}Cd_{0.5}S/1$  wt% NPBIm composite were studied by transition electron microscopy (TEM) and displayed in Figure 2. The NPBIm molecule reveals a nanosheet-like structure (Figure 2a). It can be found that, the solid solution of pure  $Zn_{0.5}Cd_{0.5}S$  sample shows irregular nanoparticles

structure (Figure 2b), and the morphology of the  $Zn_{0.5}Cd_{0.5}S/NPBIm$  hybrid photocatalyst remains unchanged (Figure 2c). This phenomenon confirms that the introduction of NPBIm molecule does not affect the crystal phase and the morphology of  $Zn_{0.5}Cd_{0.5}S$ , which is consistence with the XRD results.

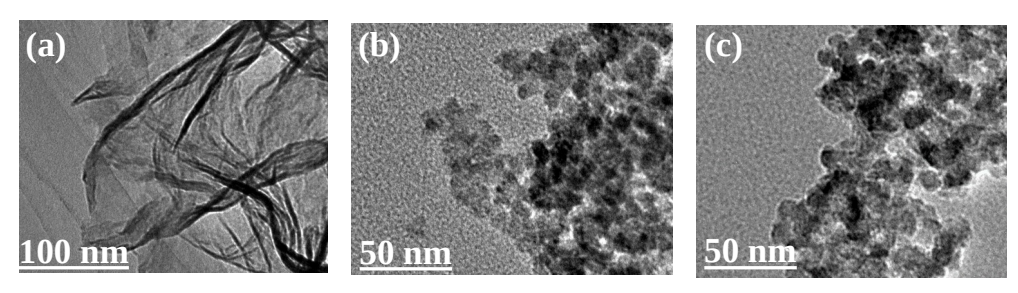


**Figure 2:** TEM images of (a) NPBIm molecule (b) pure Zn<sub>0.5</sub>Cd<sub>0.5</sub>S (c) Zn<sub>0.5</sub>Cd<sub>0.5</sub>S/1 wt% NPBIm photocatalyst.

The X-ray photoelectron spectroscopy (XPS) test was performed to investigate the chemical state and composition of NPBIm,  $Zn_{0.5}Cd_{0.5}S$  and  $Zn_{0.5}Cd_{0.5}S/NPBIm$  composite. It can be clearly seen from Figure 3a that the  $Zn_{0.5}Cd_{0.5}S/1$  wt% NPBIm composite shows the existence of Zn, Cd, S, Ni, C and N elements. The high resolution

XPS spectra of Zn 2p and Cd 3d (Figure 3b and 3c) show the binding energies of 1021.7 eV (Zn 2p<sub>3/2</sub>), 1044.8 eV (Zn 2p<sub>1/2</sub>), 405.5 eV (Cd 3d<sub>5/2</sub>) and 411.7 eV (Cd 3d<sub>3/2</sub>), which are ascribed to the Zn<sub>0.5</sub>Cd<sub>0.5</sub>S molecular environment and are in line with the previous reports for Zn<sup>2+</sup> and Cd<sup>2+</sup> (Bai et al. 2021, Lei et al. 2022 and Shen et al. 2017). The XPS

spectrum of S 2p (Fig. 3d) displays two obvious peaks located at 161.6 eV and 162.7 eV, which can be assigned that S2- is the dominant oxidation state in the sample (Lei et al. 2022). The high-resolution spectrum of N1s show peaks centered at 398.9 eV and 401.3 eV result from sp<sup>2</sup>-hybridized N atoms in C-N=C group and -NH<sub>2</sub> functional groups, respectively (Figure 3e). The peak at 404.4 eV confirms the presence of  $\pi$ - $\pi$  excitation of the C-N conjugated structure in PBIm molecule (Lei et al. 2022). High-resolution XPS spectrum of Ni 2p in Zn<sub>0.5</sub>Cd<sub>0.5</sub>S/1 wt% NPBIm heterostructured photocatalyst (Figure 3f) shows a strong peak for Ni 2p<sub>3/2</sub> and a minor peak for Ni 2p<sub>1/2</sub> at the binding energy of 855.91 eV and 873.5 eV, respectively. The peak of Ni is ascribed to the presence of Nickel (II) ion in  $Zn_{0.5}Cd_{0.5}S/1$  wt % NPBIm heterostructured photocatalyst, which is consistent with the values reported in previous works (Gan et al. 2021 and Kombo et al. 2020). Moreover, there are two satellite peaks appeared in the Ni 2p spectra, and mostly arises due to multiple splitting in the energy level of transition metals which is used to approve the existence of Nickel (II) ion (Figure 3f). Based on the above XPS results, it can be concluded that there is successful introduction of NPBIm molecule on the surface of  $Zn_{0.5}Cd_{0.5}S$  photocatalyst.

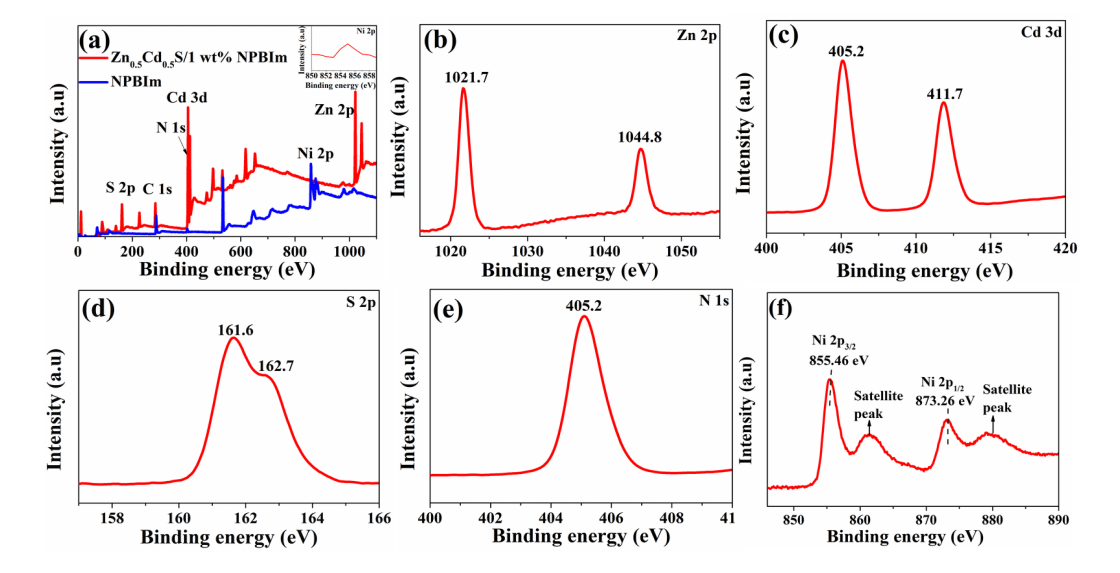


**Figure 3:** (a) XPS survey spectra of NPBIm molecule,  $Zn_{0.5}Cd_{0.5}S$  and  $Zn_{0.5}Cd_{0.5}S/1$  wt% NPBIm photocatalysts; High resolution XPS spectra of (b) Zn 2p (c) Cd 3d (d) S 2p (e) N 1s (f) Ni 2p of  $Zn_{0.5}Cd_{0.5}S/1$  wt% NPBIm photocatalyst.

Generally, the optical absorption property of a photocatalyst plays a significant role in the photocatalytic performance. Basically, the remarkable light absorption usually leads to higher photocatalytic performance of  $H_2$  evolution activity (Kombo et al. 2020 and Tahir et al. 2022). In this study, the UV-vis diffuse reflectance spectra (DRS) were measured to analyze the optical absorption properties of pristine  $Zn_{0.5}Cd_{0.5}S$ , NPBIm molecule and the as-prepared  $Zn_{0.5}Cd_{0.5}S/1$  wt

% NPBIm composite photocatalysts. As shown in Figure 4a, pure Zn<sub>0.5</sub>Cd<sub>0.5</sub>S absorbs visible light with an absorption edge of about 521 nm, and NPBIm nanosheets display strong and wide absorption in the UV-vis light regions from 300 to 800 nm. This is associated with the conjugated  $\pi$ -system of benzimidazole ligand (Kombo et al. 2020). Compared with pristine  $Zn_0 {}_5Cd_0 {}_5S$ ,  $Zn_{0.5}Cd_{0.5}S/1$ wt% **NPBIm** composite photocatalyst shows an obvious enhanced

light absorption in the visible light region, indicating that the introduction of NPBIm molecule on  $Zn_{0.5}Cd_{0.5}S$  make the photocatalyst utilize visible light more effectively, which is beneficial for enhancing photocatalytic performance of

 $Zn_{0.5}Cd_{0.5}S/NPBIm$  composite. Furthermore, the band gap energies ( $E_g$ ) of NPBIm molecule and  $Zn_{0.5}Cd_{0.5}S$  solid solution can be estimated from Kubelka-Munk method (Figure 4b), these energies are about 2.22 and 2.38 eV, respectively.

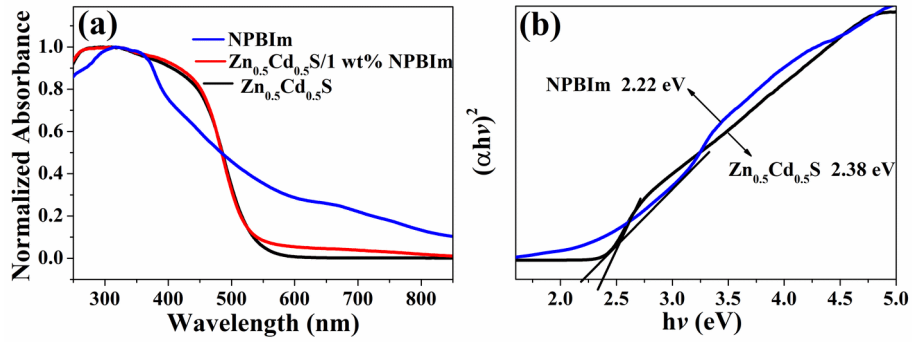


**Figure 4:** (a) UV-vis diffuse reflectance spectra of solid NPBIm,  $Zn_{0.5}Cd_{0.5}S$  and  $Zn_{0.5}Cd_{0.5}S/1$  wt% NPBIm samples (b) Energy band gap evaluation from the plots of  $(\alpha hv)^2 vs$  the energy of the absorbed light (hv) of the samples.

Moreover, the conduction band (CB) edge position plays an important part for the effective photocatalytic activities for hydrogen production. The more negative the CB edge level is, the stronger the reduction

power of a photocatalyst will be. To determine the band structure of  $Zn_{0.5}Cd_{0.5}S$  semiconductor, the Mott-Schottky plots was employed (Figure 5).

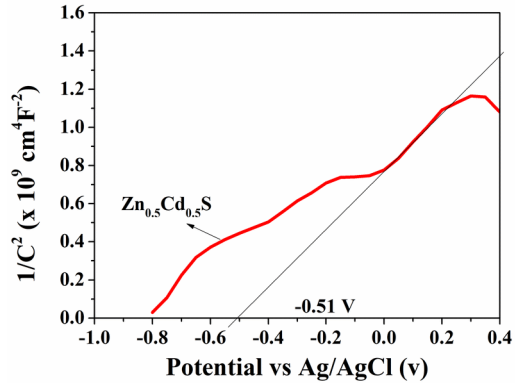


**Figure 5:** Mott-Schottky plot of Zn<sub>0.5</sub>Cd<sub>0.5</sub>S samples at 1 Hz.

The flat band potential  $(E_{fb})$  for sample calculated  $Zn_{0.5}Cd_{0.5}S$ is intercepting the extrapolation of  $1/C^2 = 0$ . The  $E_{fb}$  of  $Zn_{0.5}Cd_{0.5}S$  is estimated to be -0.51 V vs Ag/AgCl electrode, which is equal to -0.31 V vs a normal hydrogen electrode  $Zn_{0.5}Cd_{0.5}S$ sample (NHE). is n-tvpe semiconductor photocatalyst due to the positive slopes of Mott-Schottky curve. Generally, the conduction band potential  $(E_{CB})$  is about 0.1 more negative than the  $E_{fb}$  for many n-type semiconductors (Yousaf et al. 2023). Consequently,  $E_{CB}$  for  $Zn_{0.5}Cd_{0.5}S$  can be approximately determined as -0.41 V, and their valence band potential  $(E_{VB})$  is estimated to be 1.97 V. Moreover, the VB edge position of NPBIm was determined to be +0.88 eV from the valence band X-ray

photoelectron spectroscopy (VB-XPS) as shown in Figure 6. Combine with the VB-XPS value and the band gap plot data (Figure

4b) of NPBIm molecules, the CB position of NPBIm was determined to be -1.34 eV.

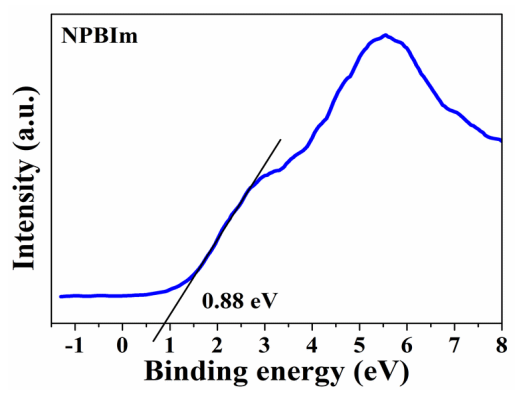


**Figure 6:** Valence band XPS spectrum of NPBIm molecule.

Generally. separation efficiency of photogenerated charge carriers plays a vital role in the photocatalytic activity of the samples. In order explore the transport, and recombination migration of photogenerated charge carriers of Zn<sub>0.5</sub>Cd<sub>0.5</sub>S and Zn<sub>0.5</sub>Cd<sub>0.5</sub>S/NPBIm nanocomposites, the steady-state photoluminescence (PL) spectra, time-resolved photoluminescence (TRPL) spectra were carried out in this study (Figure 7). Photoluminescence (PL) spectroscopy is a technique for evaluating kev recombination behavior of photogenerated charge carriers in photocatalysts. A lower PL intensity typically indicates suppressed recombination of electron-hole pairs, which correlates with improved photocatalytic activity (Kombo et al. 2020 and Tahir et al. 2022). Quantitatively, the PL peak intensity of Zn<sub>0.5</sub>Cd<sub>0.5</sub>S/NPBIm decreased relative to the pure sample. Correspondingly, the H<sub>2</sub> evolution rate increased from 92.54 µmol h-1 (pure  $Zn_{0.5}Cd_{0.5}S$ ) to 272.22 µmol  $h^{-1}$ (Zn<sub>0.5</sub>Cd<sub>0.5</sub>S/NPBIm), indicating nearly a threefold enhancement. This inverse relationship between PL intensity and H<sub>2</sub> production suggests that reduced radiative recombination contributes significantly to the increased photocatalytic efficiency. strong correlation reinforces the effectiveness of heterojunction formation in improving charge separation and overall performance. Moreover, time-resolved photoluminescence (TRPL) spectroscopy was measured to provide additional information about the charge transport and recombination process between Zn<sub>0.5</sub>Cd<sub>0.5</sub>S and NPBIm molecules. As displayed in Figure 7b, pure Zn<sub>0.5</sub>Cd<sub>0.5</sub>S shows the fluorescence lifetimes ( $\tau_1$ ) of 1.42  $\pm$  0.05 ns while Zn<sub>0.5</sub>Cd<sub>0.5</sub>S/1 wt% NPBIm composite photocatalyst exhibits a longer fluorescence lifetime ( $\tau_1$ ) of 2.30  $\pm$  0.176 ns. The longer lifetime elucidates the rapid transfer of photogenerated charge carriers in  $Zn_0 \, _5Cd_0 \, _5S/1$ wt% NPBIm composite photocatalyst, hence retarding the electronholes recombination (Tahir et al. 2022). The above PL and TRPL results suggest that Zn<sub>0.5</sub>Cd<sub>0.5</sub>S/NPBIm composite can offer more opportunities for photogenerated electrons to participate in H<sub>2</sub> evolution reaction than pure  $Zn_0 \, _5Cd_0 \, _5S$ .

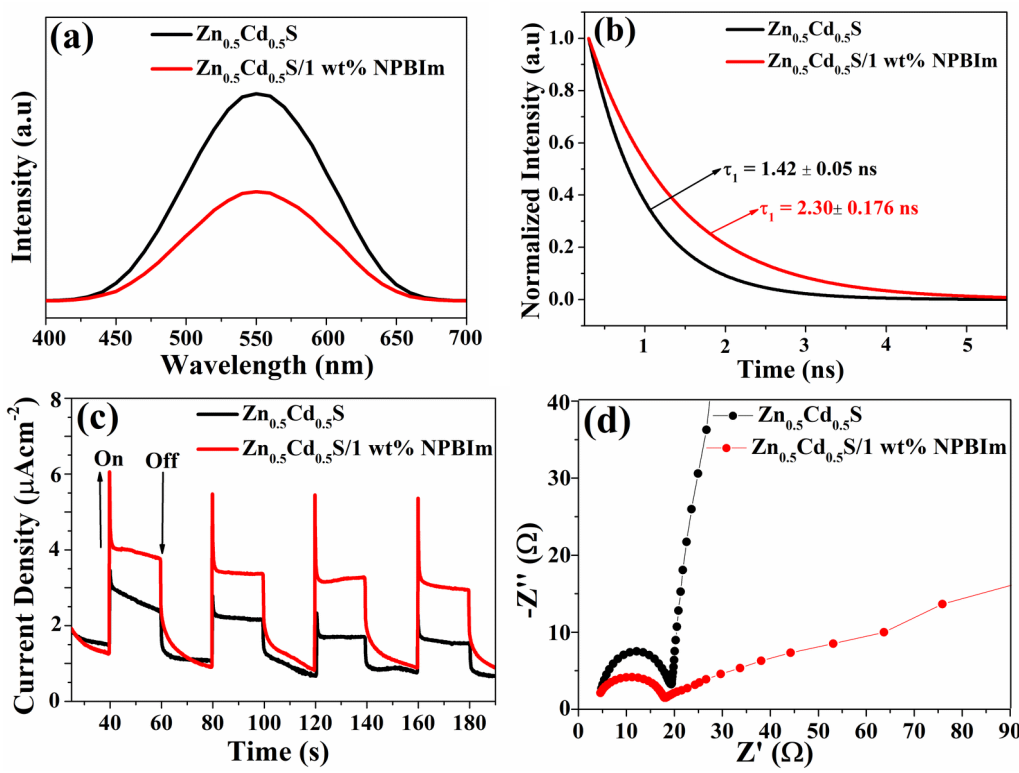
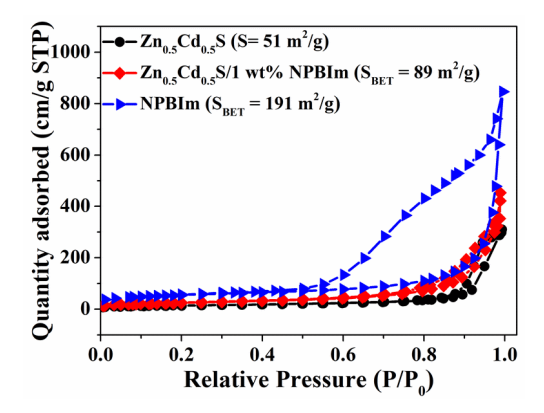


**Figure 7:** (a) Steady-state PL spectra (b) Steady-state photoluminescence time-resolved PL spectra (excitation at 325 nm, emission at 450 nm) for  $Zn_{0.5}Cd_{0.5}S$  and  $Zn_{0.5}Cd_{0.5}S/1$  wt% NPBIm photocatalyst (c) Transient photocurrent response (d) EIS Nyquist plots for  $Zn_{0.5}Cd_{0.5}S$  and  $Zn_{0.5}Cd_{0.5}S/1$  wt% NPBIm photocatalyst under visible light irradiation ( $\lambda \ge 420$  nm,  $[Na_2SO_4] = 0.5$  M).

To further support the efficient separation of photoinduced charge carriers over pure  $Zn_{0.5}Cd_{0.5}S$  and  $Zn_{0.5}Cd_{0.5}S/1$  wt% NPBIm composite photocatalyst. the photoelectrochemical tests were carried out under visible-light irradiation ( $\lambda \ge 420$  nm). Transient photocurrent responses  $Zn_{0.5}Cd_{0.5}S$  and  $Zn_{0.5}Cd_{0.5}S/1$  wt% NPBIm photocatalyst samples (Figure 7c) were carried out by typical switch on-off cycles. When the light source was turned on, the photocurrent responses of photocatalyst increases rapidly to a constant value and decreases immediately when the light was turned off. Notably, Zn<sub>0.5</sub>Cd<sub>0.5</sub>S/1wt% NPBIm composite photocatalyst exhibited about 1.9 times higher intensity than pure Zn<sub>0.5</sub>Cd<sub>0.5</sub>S. extremely enhanced photocurrent response manifesting a better separation efficiency and lower recombination rate of photoinduced charge carriers in Zn<sub>0.5</sub>Cd<sub>0.5</sub>S/NPBIm (Gan et al. 2021 and Kombo 2020). addition, et al. electrochemical impedance spectroscopy (EIS) can also be used to elucidate the interface charge separation efficiency. Generally, it is believed that the smaller arc radius represents an efficient separation of photogenerated charge carriers and a fast interface charge transfer process (Yousaf et al. 2023). As displayed in Figure 7d, the composite  $(Zn_{0.5}Cd_{0.5}S/1$ wt% NPBIm) sample exhibits a smaller arc radius than that of  $Zn_{0.5}Cd_{0.5}S$ , suggesting the  $Zn_{0.5}Cd_{0.5}S/1$  wt NPBIm has more efficient carrier separation capability (Kombo et al. 2020 and Yousaf et al. 2023). The photoelectrochemical results are consistent with the PL and TRPL spectroscopy. Taken

together, the  $Zn_{0.5}Cd_{0.5}S/NPBIm$  composite is an appealing photocatalyst.

Furthermore, the surface area of the catalyst plays a critical role in enhancing photocatalytic activity. Samples exhibiting areas generally higher surface increased H<sub>2</sub> production rates, indicating that a larger number of active sites facilitates photocatalysis (Kombo et al. 2020). To evaluate this Nitrogen adsorption-desorption isotherm were used to determine the BET specific surface areas (SBET) of samples. The measured (SBET) values for NPBIm molecule, pure  $Zn_{0.5}Cd_{0.5}S$  and  $Zn_{0.5}Cd_{0.5}S/1$ NPBIm composite were 191 m<sup>2</sup> g<sup>-1</sup>, 51 m<sup>2</sup> g<sup>-1</sup> and 89 m<sup>2</sup> g<sup>-1</sup>, respectively, as shown in Figure 8. Notably, the  $Zn_{0.5}Cd_{0.5}S/1$  wt% NPBIm composite exhibited a significantly higher surface area than pure Zn<sub>0.5</sub>Cd<sub>0.5</sub>S, correlating with an increase in photocatalytic hydrogen production rate from 92.54 µmol h<sup>-1</sup> (pure  $Zn_{0.5}Cd_{0.5}S$ ) to 272.22 µmol  $h^{-1}$  $(Zn_{0.5}Cd_{0.5}S/NPBIm).$ This threefold enhancement aligns with the ~75% increase in surface area, supporting the hypothesis that increased surface area improves the number of active sites, enhances charge carrier transport, and ultimately boosts photocatalytic performance. This statistical correlation reinforces the importance of optimizing surface properties in the design of high-efficiency photocatalysts.



Na<sub>2</sub>SO<sub>3</sub> under visible light irradiation ( $\lambda \ge 420$  nm) (Figure 9).

**Figure 8:** Nitrogen adsorption-desorption isotherms of NPBIm molecule, pure  $Zn_{0.5}Cd_{0.5}S$  and  $Zn_{0.5}Cd_{0.5}S/1$  wt% NPBIm composite.

All the above results indicate the  $Zn_{0.5}Cd_{0.5}S/NPBIm$  composites have fast charge carriers transfer rate, high surface area, excellent optical and electronic properties, which are certainly favorable to promote the photocatalytic activity. The  $H_2$  evolution rates of  $Zn_{0.5}Cd_{0.5}S/NPBIm$  composite photocatalysts with different amounts of NPBIm loadings are tested by using 100 mL of aqueous solution containing 0.15 M  $Na_2S$  and 0.15 M

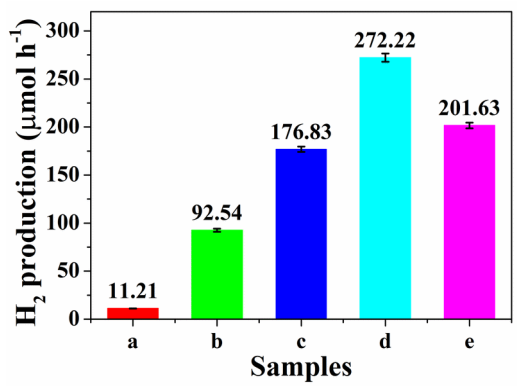


**Figure 9:** Visible light photocatalytic performances of different samples. (a) NPBIm, (b)  $Zn_{0.5}Cd_{0.5}S$ , (c)  $Zn_{0.5}Cd_{0.5}S/0.5$  wt% NPBIm (d)  $Zn_{0.5}Cd_{0.5}S/1$  wt% NPBIm (e)  $Zn_{0.5}Cd_{0.5}S/1.5$  wt% NPBIm: Reaction conditions: 0.05 g of photocatalyst; 100 mL of aqueous solution with 0.15 M Na<sub>2</sub>S.9H<sub>2</sub>O and 0.15 M Na<sub>2</sub>SO<sub>3</sub>; light source, 300 W xenon lamp (λ ≥ 420 nm), at 10 °C.

When Zn<sub>0.5</sub>Cd<sub>0.5</sub>S used as photocatalyst alone, the H<sub>2</sub> production rate is only 92.54 umol h<sup>-1</sup>. The small rate of H<sub>2</sub> production is attributed by the rapid recombination rate of photogenerated electron-hole pairs (Figure 9b). Noticeably, only small amount of H<sub>2</sub> was detected when NPBIm alone was used as the catalyst under the same experimental conditions (Figure 9a). As expected, the hydrogen efficiency of photocatalytic evolution of Zn<sub>0.5</sub>Cd<sub>0.5</sub>S was significantly enhanced (Fig. 9c-e) when NPBIm was introduced to the surface. It's worth noting that the photocatalytic H<sub>2</sub> production activity of Zn<sub>0.5</sub>Cd<sub>0.5</sub>S/NPBIm composites largely depends on the loading amount of NPBIm molecule. And an optimal H<sub>2</sub> evolution rate could be obtained (272.22 µmol h<sup>-1</sup>) when loading amount of NPBIm increased to 1 wt % (Figure 9d), which is 3 times higher than that of Zn<sub>0.5</sub>Cd<sub>0.5</sub>S alone. It is also comparatively higher to other Zn<sub>0.5</sub>Cd<sub>0.5</sub>S-

based heterostructure photocatalyst reported in previous studies (Table 1). However, further increase of NPBIm content to 1.5 wt % in the metal complex/semiconductor hybrid photocatalyst leading to a dramatic deterioration of hydrogen evolution rate (Figure 9e). The possible reason is that excess NPBIm molecule could result a shielding effect on the incident light to reach the surface of Zn<sub>0.5</sub>Cd<sub>0.5</sub>S photocatalyst (Kombo et al. 2019). On the other hand, the excess NPBIm molecule would reduce the active sites of Zn<sub>0.5</sub>Cd<sub>0.5</sub>S, which further decreasing the photocatalytic activity of Zn<sub>0.5</sub>Cd<sub>0.5</sub>S/NPBIm composite (Kombo et al. 2020). It can be concluded that, therefore, loading an appropriate amount of NPBIm molecules onto Zn<sub>0.5</sub>Cd<sub>0.5</sub>S is a crucial step for optimizing the photocatalytic activity of Zn<sub>0.5</sub>Cd<sub>0.5</sub>S/NPBIm composite for hydrogen evolution.

Miza Kombo et al. - Nickel (II) Complex Decorated Zinc-Cadmium Sulfide Type-II Heterojunction for Enhanced Photocatalytic Hydrogen Production

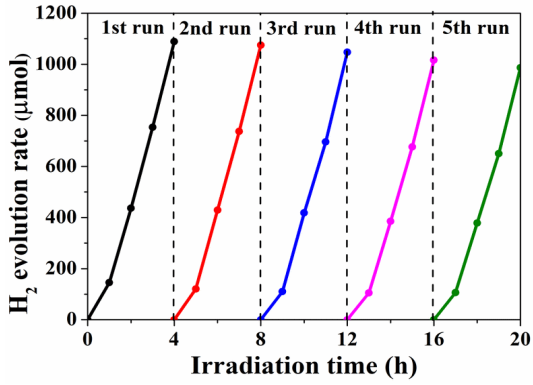
**Table 1.** Comparison of photocatalytic activities for hydrogen production various composite

based on Zn<sub>0.5</sub>Cd<sub>0.5</sub>S reported previously.

Photocatalyst	Light source	Sacrificial reagent	HER μmolh <sup>-1</sup> g <sup>-1</sup>	Refs.
Zn <sub>0.5</sub> Cd <sub>0.5</sub> S/ NPBIm	300 W Xe-lamp λ ≥ 420 nm	0.15M Na <sub>2</sub> S+0.15 M Na <sub>2</sub> SO <sub>3</sub>	5444	This work
$Zn_{0.5}Cd_{0.5}S/$ $MoO_2$	300 W Xe-lamp λ ≥ 420 nm	0.1 M Na <sub>2</sub> S+0.1 M Na <sub>2</sub> SO <sub>3</sub>	2524	(Du et al. 2015)
$Zn_{0.5}Cd_{0.5}S/$ $BiVO_4$	300 W Xe-lamp λ > 420 nm	0.35M Na <sub>2</sub> S+ 0.25 M Na <sub>2</sub> SO <sub>3</sub>	2350	(Zeng et al. 2018)
$Zn_{0.5}Cd_{0.5}S/$ $MoS_2$	500 W Tungsten- halogen lamp	0.1M Na <sub>2</sub> S+0.1 M Na <sub>2</sub> SO <sub>3</sub>	2450	(Gogoi et al. 2018)
$Zn_{0.5}Cd_{0.5}S-g-$ $C_3N_4-MoS_2$	500 W Tungsten- halogen lamp	0.1M Na <sub>2</sub> S+0.1 M Na <sub>2</sub> SO <sub>3</sub>	4565	(Gogoi et al. 2018)
$\begin{array}{c} Ni_2P/\\ Zn_{0.5}Cd_{0.5}S \end{array}$	300 W Xe-lamp λ ≥ 420 nm	0.25 M Na <sub>2</sub> S+ 0.35 M Na <sub>2</sub> SO <sub>3</sub>	1312	(Peng et al.2018)
Zn <sub>0.5</sub> Cd <sub>0.5</sub> S/ CdS QDs	350 W Xe-lamp λ > 400 nm	0.1 M Na <sub>2</sub> S+0.04 M Na <sub>2</sub> SO <sub>3</sub>	2128	(Ran et al. 2011)
Zn <sub>0.5</sub> Cd <sub>0.5</sub> S/ Graphene	150 W Xe-lamp λ ≥ 400 nm	0.35 M Na <sub>2</sub> S+ 0.25 M Na <sub>2</sub> SO <sub>3</sub>	1060	(Li et al. 2014)
Pt-RuS <sub>2</sub> - Zn <sub>0.5</sub> Cd <sub>0.5</sub> S	Day-light fluorescent lamp	0.6 M Na <sub>2</sub> S+0.8 M Na <sub>2</sub> SO <sub>3</sub>	4550	(Gaikwad et al. 2016)
AuPd/Zn <sub>0.5</sub> Cd <sub>0.5</sub> S	300 W Xe lamp-λ ≥ 400 nm	0.44 M Na <sub>2</sub> S+ 0.31 M Na <sub>2</sub> SO <sub>3</sub>	3650	(Wu et al.2016)

Excellent photocatalytic performances of hydrogen production, in combination with its recycling performance signify significant practical application. The stability and recycling performance of the photocatalyst were tested by running hydrogen evolution experiments repeatedly five times by using Zn<sub>0.5</sub>Cd<sub>0.5</sub>S/1 wt% NPBIm composite under

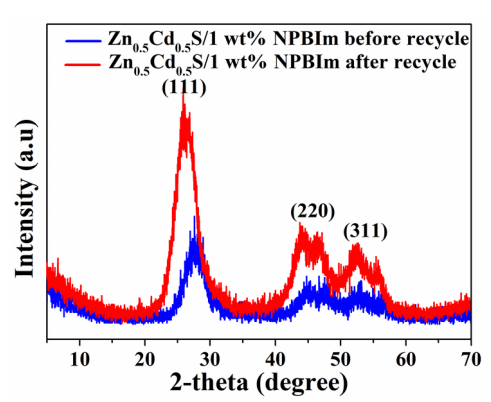
the same reaction conditions. As displayed in Figure 10, after five successive runs, the catalyst does not exhibit obvious loss of photocatalytic activity. This infers an excellent stability of  $Zn_{0.5}Cd_{0.5}S/1$  wt% NPBIm composite during photocatalytic hydrogen production.



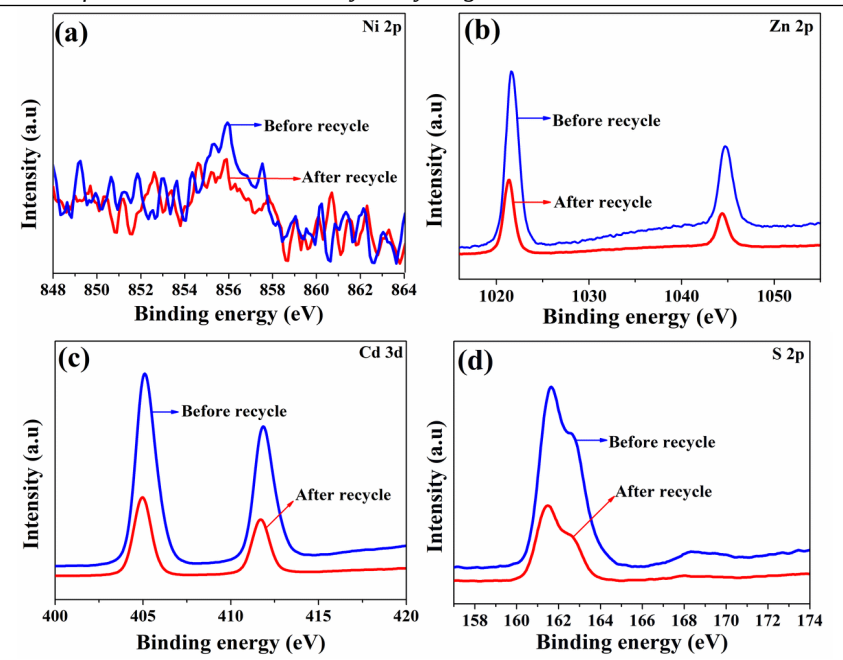
**Figure 10:** The reusability tests of  $Zn_{0.5}Cd_{0.5}S/1$  wt% NPBIm photocatalyst for photocatalytic hydrogen production. Reaction conditions: 0.05 g of photocatalyst; 100 mL of aqueous solution with 0.15 M  $Na_2S.9H_2O$  and 0.15 M  $Na_2SO_3$ ; light source, 300 W xenon lamp ( $\lambda \ge 420$  nm), at 10 °C ( $H_2$  produced was evacuated after every 4 h).

Figure 11 and Figure 12 depict XRD pattern and high-resolution XPS spectra of Ni 2p, Zn 2p, Cd 3d, and S 2p for the Zn<sub>0.5</sub>Cd<sub>0.5</sub>S/1 wt% NPBIm sample before and after the photocatalytic recycling tests, respectively. The results demonstrate that there are no remarkable changes for

 $Zn_{0.5}Cd_{0.5}S/1$  wt% NPBIm hybrid photocatalyst before and after the stability analysis, further ratifies that  $Zn_{0.5}Cd_{0.5}S/NPBIm$  composite photocatalyst possesses a satisfactory stability, and has a great potential in photocatalytic practical application.



**Figure 11:** XRD spectra of Zn<sub>0.5</sub>Cd<sub>0.5</sub>S/1 wt% NPBIm composite photocatalysts before and after recycle.



**Figure 12:** High-resolution XPS spectra of (a) Ni 2p, (b) Zn 2p, (c) Cd 3d, (d) S 2p for Zn<sub>0.5</sub>Cd<sub>0.5</sub>S/1 wt% NPBIm composite photo catalysts before and after recycle.

On the basis of above research and analysis, a possible type-II mechanism on Zn<sub>0.5</sub>Cd<sub>0.5</sub>S/NPBIm heterostructure is proposed and illustrated in Figure 13. This Figure depicts more negative value of CB and VB energy level for NPBIm as compared to that of  $Zn_{0.5}Cd_{0.5}S$ . As a result, type-II heterojunction of Zn<sub>0.5</sub>Cd<sub>0.5</sub>S/NPBIm formed (Kombo et al. 2019). Therefore, owing the presence of suitable band gaps, both Zn<sub>0.5</sub>Cd<sub>0.5</sub>S and NPBIm can be excited simultaneously to produce the photoinduced charge carriers under visible-light irradiation. The photogenerated electrons in the CB of NPBIm are quickly transferred to the CB of  $Zn_{0.5}Cd_{0.5}S$  across their interface, and the holes at the valence band of  $Zn_{0.5}Cd_{0.5}S$  can migrate to the VB of NPBIm. The accumulated photoinduced electrons on the surface of  $Zn_{0.5}Cd_{0.5}S$  will reduce the water molecules to hydrogen gas; simultaneously, the holes in NPBIm are consumed by the sacrificial agent ( $S^2$ -,  $SO_3^2$ -). This event facilitates an effective separation between photoinduced electrons and holes in a system. Consequently, the photocatalytic hydrogen production activity of  $Zn_{0.5}Cd_{0.5}S/NPBIm$  composites is boosted.

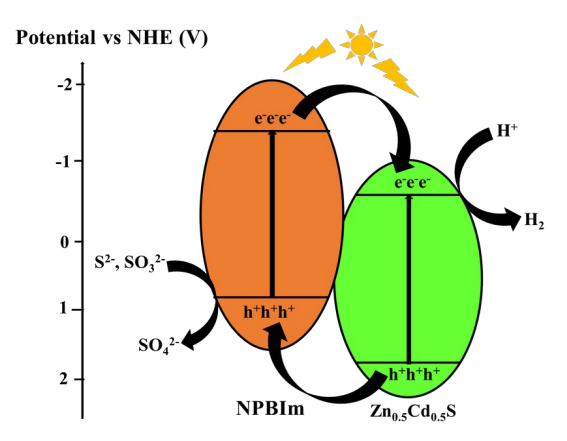


**Figure 13:** Energy-level diagram and charge transfer processes for Zn<sub>0.5</sub>Cd<sub>0.5</sub>S/NPBIm type-II heterostructured photocatalyst under visible light irradiation.

### Conclusions

In summary, a novel heterostructured photocatalyst for hydrogen generation was developed by introducing nickel (II)-(3pyridyl) benzimidazole (NPBIm) complexes on the surface of Zn<sub>0.5</sub>Cd<sub>0.5</sub>S. This metal complex semiconductor photocatalysts effectively inhibits the recombination of photogenerated electrons and holes through spatial charge separation. Under the optimal experimental conditions, the  $Zn_0 \, _5Cd_0 \, _5S/1$  wt % NPBIm composite photocatalyst exhibits the highest photocatalytic hydrogen activity (272.22 µmol h<sup>-1</sup>) under visible light irradiation ( $\lambda \geq 420$  nm), tripling the performance of pure  $Zn_{0.5}Cd_{0.5}S$ . Zn<sub>0.5</sub>Cd<sub>0.5</sub>S/NPBIm Additionally. the photocatalyst demonstrates stable hydrogen production over 20 hours, suggesting that the **NPBIm** complex molecule protects Zn<sub>0.5</sub>Cd<sub>0.5</sub>S from photo-corrosion. This work offers newperspectives for designing metalcomplex semiconductor systems photocatalytic applications.

## **Conflicts of Interest:**

The authors declare no conflict of interest.

### Acknowledgements

The authors gratefully acknowledge the special funding support from the National Natural Science Foundation of China (51572253, 21771171), and a Scientific Research Grant of Hefei National Synchrotron Radiation Laboratory (UN 2017LHJJ), the Fundamental Research Funds

for the Central Universities (YD2340002001). This work is also supported by CSC fellowship program.

#### References

Bai T, Shi X, Liu M, Huang H, Zhang J and Bu X 2021 g-C<sub>3</sub>N<sub>4</sub>/ZnCdS heterojunction for efficient visible light-driven photocatalytic hydrogen production. *RSC Adv.* 38120–38125.

Chen H, Zhu Y, Wu J ,Peng M, Deng S, Yang H and Yang J 2024 Cu-doped ZnCdS-based photocatalyst for efficient photocatalytic hydrogen production by photothermal assistance. *Case Stud. Therm. Eng.* 61:104970.

Du H, Xie X, Zhu Q, Lin L, Jiang YF, Yang ZK, Zhou X and Xu AW 2015 Metallic  $MoO_2$  cocatalyst significantly enhances visible-light photocatalytic hydrogen production over  $MoO_2/Zn_{0.5}Cd_{0.5}S$  heterojunction. *Nanoscale*. 7(13): 5752–5759.

Fujishima A and Honda K 1992 Electrochemical Photolysis of water at a Semiconductor Electrode. *Nature*. 238: 37–38.

Gan S, Deng M, Hou D, Huang L, Qiao XQ and Li DS 2021 An amorphous  $NiS_X$  film as a robust cocatalyst for boosting photocatalytic hydrogen generation over ultrafine ZnCdS nanoparticles. *Mater. Adv.* 2(12): 3881–3891.

Geng JC, Qin L, Du X, Xiao SL and Cui GH

- 2012 Synthesis, crystal structures, and catalytic properties of silver(I) and cobalt(II) coordination polymers based on flexible bis(benzimidazole) with pyridine-2, 6-dicarboxylate. *Z.Fur. Anorg. Allg. Chem.* 638(7–8): 1233–1238.
- Grushevskaya S, Belyanskaya I and Kozaderov O 2022 Approaches for Modifying Oxide-Semiconductor Materials to Increase the Efficiency of Photocatalytic Water Splitting. *Mater*. 15:4915.
- Hamdan S, Al-Ali K, Vega LF, Muscetta M, Yusuf AO and Palmisano G 2024 Zinc cadmium sulphide (Zn<sub>x</sub>Cd<sub>1-x</sub>S)-based photocatalysts for hydrogen production from seawater and wastewater. *J. Environ. Chem. Enq.* 12(5): 113937.
- Icli S, Zafer C, Ulusoy M, Dittrich T, Ozsoy C, Cetinkaya B, Varlikli C and Sahin C 2009 The synthesis and characterization of 2-(2'-pyridyl)benzimidazole heteroleptic ruthenium complex: Efficient sensitizer for molecular photovoltaics. *Dyes. Pigm.* 84(1): 88–94.
- Kombo M, Chong HB, Ma LB, Sahar S, Fang XX, Zhao T, Ling C, Lu XJ and Xu AW 2020 Graphitic Carbon Nitride Decorated with Nickel(II)-(3-Pyridyl) Benzimidazole Complexes and Pt Nanoparticles as a Cocatalyst for Photocatalytic Hydrogen Production from Water Splitting. ACS Appl. Nano Mater. 3(11): 10659–10667.
- Kombo M, Ma LB, Liu YN, Fang XX, Ullah N, Odda AH and Xu AW 2019 Graphitic carbon nitride/CoTPP type-II heterostructures with significantly enhanced photocatalytic hydrogen evolution. *Catal. Sci. Technol.* 9(9): 2196–2202.
- Lei Y, Zhang Y, Li Z, Xu S, Huang J, Hoong NK and Lai Y 2021 Molybdenum sulfide cocatalyst activation upon photodeposition of cobalt for improved photocatalytic hydrogen production activity of ZnCdS. *Chem.Eng.J.* 425: 131478.
- Mamiyev Z and Balayeva NO 2022 Metal Sulfide Photocatalysts for Hydrogen Generation: A Review of Recent

- Advances. Catal. 12(11): 1-36.
- Qi S, Miao Y, Chen J, Chu H, Tian B, Wu B, Li Y and Xin B 2021 Controlled biosynthesis of zncds quantum dots with visible-light-driven photocatalytic hydrogen production activity. Nanomaterials. 11(6): 1357.
- Shen CC, Liu YN, Zhou X, Guo HL, Zhao ZW, Liang K and Xu AW 2017 Large improvement of visible-light photocatalytic  $H_2$  evolution based on cocatalyst-free  $Zn_{0.5}Cd_{0.5}S$  synthesized through a two-step process. *Catal. Sci.Technol.* 7(4): 961–967.
- Su C, Yang X, Liao S, Mak TC and Kang BS 1999 Anion-controlled assembly of low-dimensional silver(I) complexes of 2-(3-pyridyl) benzimidazole (PyBIm). *Inorg. Chem. Commun.* 2: 383–385.
- Tahir W, Cheang TY, Li JH, Ling C, Lu XJ, Ullah I, Wang G and Xu AW 2022 Interfacial Ti≡N bonding of a g-C<sub>3</sub>N<sub>4</sub>/TiH<sub>1.92</sub> type-II heterojunction photocatalyst significantly enhanced photocatalytic hydrogen evolution from water splitting. *Catal. Sci.Technol.* 12(6): 2023–2029.
- Tahir W, Ullah S, Ullah I Li JH, Ling C, Lu XJ, Qian XJ, Wang G, Pan Y and Xu AW 2022 Metallic WN plasmonic fabricated g-C<sub>3</sub>N<sub>4</sub> significantly steered photocatalytic hydrogen evolution under visible and near-infrared light. *Catal. Sci.Technol.* 12(24): 7369–7378.
- Wei ML, Wang YX and Wang XJ 2014 Two proton-conductive hybrids based on 2-(3-pyridyl)benzimidazole molecules and Keggin-type heteropolyacids. *J. Solid State Chem.* 209: 29–36.
- Yousaf A, BinImran M Farooq M, Kausar S, Yasmeen S and Kasak P 2023 Graphitic Carbon Nitride Nanosheets Decorated with Zinc-Cadmium Sulfide for Type-II Heterojunctions for Photocatalytic Hydrogen Production. *Nanomaterials*. 13(18).
- Yuan H, Fang F, Dong J, Xia W, Zeng X and Shangguan W 2022 Enhanced photocatalytic hydrogen production based on laminated MoS<sub>2</sub>/g-C<sub>3</sub>N<sub>4</sub> photocatalysts. *Colloids Surf. A: Physicochem. Eng. Asp.*

641: 128575.